20th International Conference on Structural Mechanics in Reactor Technology (SMiRT 20)
Espoo, Finland, August 9-14, 2009
SMiRT 20-Division III, Paper 1909

An evaluation of methods for the time-domain simulation of turbulence excitations for tube bundles subjected to non-uniform flows

Jose Antunes[a], Philippe Piteau[b], Xavier Delaune[b], Laurent Borsoi[b]

[a] *Instituto Tecnológico e Nuclear (ITN), Applied Dynamics Laboratory (ADL)*
Sacavem, Portugal, e-mail: jantunes@itn.pt
[b] *Commissariat a l'Energie Atomique (CEA), DM2S/SEMT/DYN Laboratory*
Saclay, France

Keywords: Flow-induced vibration, Turbulence modelling, Tube bundles, Heat exchangers, Steam generators.

1 ABSTRACT

The present paper addresses the problem of achieving adequate modelling of the turbulence excitations, when performing nonlinear time-domain computations for the predictive dynamical analysis of gap-supported tube bundles of nuclear power-plant components – namely steam generators. Although in most publications the details on time-domain implementations of turbulence excitations are seldom supplied, it is a nontrivial task to provide adequate time-domain force functions which rightly account for the spectral properties, the space correlation, as well as the local magnitude of the flow velocity field. Oversimplified approaches may lead to inadequate modelling of the excitation, and hence to unreliable predictive results.

We recently proposed a simple and consistent method to simulate the continuous space-correlated flow force field (Antunes et al, 2008), using a finite set of uncorrelated discrete random forces, which are computed based on the theoretical formulation for the linear modal responses of the excited tube. Here we investigate whether such computationally efficient approach is effective, even when dealing with the nonlinear vibro-impact responses of gap-supported tubes subjected to non-uniform flows. Illustrative linear and nonlinear tube response computations using our simple excitation method are compared with those obtained by modelling the turbulence through a partially correlated random field, computed using the more computationally intensive techniques developed by Shinozuka et al (1971, 1990).

2 INTRODUCTION

The predictive dynamical analysis of gap-supported tubular bundles subjected to turbulence-induced vibrations is of practical significance, in particular when addressing nuclear power-plant facilities. It is a multi-disciplinary work which resulted in a number of computational tools, mostly based on time-domain numerical simulations of the flow-excited nonlinear systems – see, for instance, Sauvé and Teper (1987), Axisa et al (1988), Fisher et al (1989), Haslinger and Steininger (1995) or Hassan et al (2003). The present paper addresses the problem of achieving adequate modelling of the turbulence excitations when performing such time-domain computations.

In most published work, the details on time-domain implementations of turbulence excitations are seldom supplied, as if such modelling aspects were obvious or non-important. Actually, providing adequate time-domain force functions – which rightly account for the spectral properties, the space correlation, as well as the local magnitude of the flow velocity field – is a nontrivial task. Indeed, numerical simulations are often performed by exciting the tubes with random forces which account in a very crude manner, or even not at all, for the partial space correlation of the flow turbulence. For instance, a common approach is to excite the system through a number of random forces assuming full correlation within each tube span and none beyond – see, for instance, Hassan et al (2003). Such oversimplified approaches may lead to inadequate modelling of the excitation, and hence to unreliable predictive analysis. In the present paper, our developments addressing such issue are presented and discussed.

We recently proposed a simple but consistent method to simulate the continuous space-correlated flow force field, using a finite set of uncorrelated discrete random forces located along the structure – see Antunes et al (2008). These are computed from the turbulence spectrum and the space correlation of the original

turbulence field, accounting for the flow velocity profile, based on the theoretical formulation for the linear modal responses of the excited tube. Our approach has been validated on simple test cases, consisting on single-span and linearly multi-supported tubes. On the other hand, sample computations suggest that such computationally efficient approach is also effective when dealing with the nonlinear vibro-impact responses of gap-supported tubes subjected to non-uniform flows, as originally intended. Analysis of these essential aspects was needed and is offered in the present paper. Here, illustrative linear and nonlinear tube response computations using our simple excitation method are compared with those obtained by modelling the turbulence through a partially correlated random field, computed using the more involved and computationally intensive general techniques developed by Shinozuka (1971, 1990) and co-workers. The results presented stress the effectiveness of both techniques, as well as their merits and drawbacks in terms of computational efficiency and accuracy.

3 TUBE RESPONSES TO TURBULENT FLOW EXCITATIONS

We start by recalling the main results concerning the linear vibratory responses of tubes subjected to the turbulence excitation of cross-flows. Full details are provided in the papers by Axisa et al (1990) and Antunes et al (2008). Consider a tubular structure with length L, external diameter D and modal properties m_n, ω_n, ξ_n and $\phi_n(x)$, which is subjected to a random force field $f(x,t)$ stemming from a turbulence excitation. The flow is described by its density ρ and the velocity profile $V(x) = \bar{V}\,u(x)$, where $\bar{V}$ is a representative flow velocity and $u(x)$ the normalized velocity profile. $\bar{V}$ is obtained by averaging the velocity profile $V(x)$ within the tube length L_f subjected to the flow. Then, linear tube responses are given by the modal equations $(n = 1,2,...,N)$:

$$m_n \ddot{q}_n + 2m_n\omega_n\xi_n\dot{q}_n + m_n\omega_n^2 q_n = f_n(t) \tag{1}$$

while the physical responses $y(x,t)$ and modal forces $f_n(t)$ are computed as:

$$y(x,t) = \sum_{n=1}^{N} \phi_n(x)\, q_n(t) \quad ; \quad f_n(t) = \int_0^L \phi_n(x)\, f_y(x,t)\, dx \tag{2}$$

and similarly for the orthogonal motion $z(x,t)$ and the corresponding physical and modal forces.

Then, following the well established theory of random vibrations, the cross-spectra of the modal responses are obtained in the frequency domain as $(m = 1,2,...,N\,;\, n = 1,2,...,N)$:

$$S_{q_n q_m}(\omega) = H_n(\omega) H_m^*(\omega) \int_0^L\int_0^L \phi_n(x_1)\,\phi_m(x_2)\, S_f\left(x_1, x_2, \omega\right) dx_1 dx_2 \tag{3}$$

where $H_n(\omega) = \left[m_n\left(\omega_n^2 - \omega^2 + 2i\omega\omega_n\xi_n\right)\right]^{-1}$ and the excitation field $f_y(x,t)$ is entirely described in terms of its cross-spectrum $S_f\left(x_1, x_2, \omega\right)$. Then physical response is given by:

$$S_{yy}(x,\omega) = \sum_{n=1}^{N}\sum_{m=1}^{N} \phi_n(x)\,\phi_m(x)\, S_{q_n q_m}(\omega) \tag{4}$$

Often cross-terms are much smaller than the diagonal terms in (4), which then simplifies to:

$$S_{yy}(x,\omega) = \sum_{n=1}^{N} \left[\phi_n(x)\right]^2 S_{q_n q_n}(\omega) \tag{5}$$

with:

$$S_{q_n q_n}(\omega) = \left|H_n(\omega)\right|^2 \int_0^L\int_0^L \phi_n(x_1)\,\phi_n(x_2)\, S_f\left(x_1, x_2, \omega\right) dx_1 dx_2 \tag{6}$$

As is well known, the turbulence excitation $S_f\left(x_1, x_2, \omega\right)$ may be conveniently modelled in terms of a local auto-spectrum $\Phi\left(x, \omega\right)$ and a spatial correlation function $\gamma\left(x_1, x_2, \omega\right)$:

$$S_f\left(x_1, x_2, \omega\right) = \left[\Phi(x_1,\omega)\,\Phi(x_2,\omega)\right]^{1/2} \gamma\left(x_1, x_2, \omega\right) \tag{7}$$

where $\left|\gamma\left(x_1, x_2, \omega\right)\right| \le 1$ and in general is real or complex. For *cross-flow excitations*, the spatial correlation function is real and may be described in the simple form:

$$\gamma_{Tr}\left(x_1, x_2, \omega\right) = \exp\left(-\left|x_2 - x_1\right| / \lambda_c(\omega)\right) \tag{8}$$

where λ_c is a correlation length of the force fluctuations, which for tube bundles is of the order of the tube diameter – see Inada et al (2007).

For obvious reasons it is convenient to express the turbulence spectra in dimensionless form. For single-phase flows, collapsing of experimental data is achieved by scaling Φ in terms of the flow pressure head and using the reduced frequency $f_R = fD/V$, so that the following *reduced spectrum* $\bar{\Phi}$ is obtained:

$$\bar{\Phi}(f_R) = \left(\frac{1}{2}\rho V^2 D\right)^{-2} \frac{V}{D}\Phi(f) \quad ; \quad f_R = \frac{fD}{V} \tag{9}$$

and using (7) and (8), the modal tube responses (6) are given by:

$$S_{q_n q_n}(\omega) = \left|H_n(\omega)\right|^2 \int_0^L\int_0^L \phi_n(x_1)\phi_n(x_2)\left[\Phi(x_1,\omega)\Phi(x_2,\omega)\right]^{1/2} \exp\left(-\frac{\left|x_2 - x_1\right|}{\lambda_c}\right) dx_1 dx_2 \tag{10}$$

Then, accounting for (9), we obtain after some simplifying assumptions (Axisa et al, 1990):

$$S_{q_n q_n}(f) = \left(\frac{1}{2}\rho \bar{V}^2 D\right)^2 \frac{D}{\bar{V}}\left|H_n(f)\right|^2 \bar{\Phi}\left(\frac{fD}{\bar{V}}\right) L_{cn}^2 \quad ; \quad \bar{V} = \frac{1}{L_f}\int_0^{L_f} V(x)\,dx \tag{11}$$

where L_{cn} is the so-called *joint-acceptance* integral, which encapsulates the combined effects of the spatial correlation of the fluctuations λ_c, the flow velocity profile $u(x)$ and the structural modeshapes $\phi_n(x)$:

$$L_{cn}^2 = \int_0^{L_f}\int_0^{L_f} u(x_1)^2\, u(x_2)^2 \phi_n(x_1)\phi_n(x_2) \exp\left(-\frac{\left|x_2 - x_1\right|}{\lambda_c}\right) dx_1 dx_2 \approx 2\lambda_c \int_0^{L_f} \left[u(x)^2 \phi_n(x)\right]^2 dx \tag{12}$$

Because in general $\lambda_c / L_f \ll 1$, the integration can be simplified drastically, as shown in (12), so that (11) reduces to (Axisa et al, 1990):

$$S_{q_n q_n}(f) = \left(\frac{1}{2}\rho \bar{V}^2 D\right)^2 \frac{D}{\bar{V}}\left|H_n(f)\right|^2 \bar{\Phi}_E\left(\frac{fD}{\bar{V}}\right) C_n^2 \tag{13}$$

where:

$$\bar{\Phi}_E(f_R) = \frac{\lambda_c}{L_f}\bar{\Phi}(f_R) \quad ; \quad C_n^2 = 2L_f \int_0^{L_f} \left[u(x)^2 \phi_n(x)\right]^2 dx \tag{14}$$

Notice that an *equivalent spectrum* $\bar{\Phi}_E$ has been defined in (14), which embeds the effects of the correlation length λ_c. Provided that $\lambda_c / L_f \ll 1$, such formulation avoids difficulties stemming from an insufficient knowledge (or a frequency-dependence) of the correlation length λ_c.

4 GENERATION OF THE TIME-DOMAIN TURBULENCE EXCITATIONS

In this section we will briefly review the general technique implemented following Shinozuka et al (1990) to simulate the turbulence random field by generating a set of partially correlated random forces, as well as the simple method developed by Antunes et al (2008) which uses a set of uncorrelated random forces.

4.1 General method using a set of partially correlated forces

The starting point of all spectral-based methods for generating a set of P partially correlated point-forces $\{f_P(t)\}$ is the frequency-dependent excitation cross-spectrum (7). In matrix terms, let us write:

$$\begin{cases} S_f(x_i, x_j, f) \equiv S_{ij}(f) = \Delta x^2 \left[\Phi_i(f)\Phi_j(f)\right]^{1/2} \gamma_{ij}(f) \\ i, j = 1, 2, \ldots P \end{cases} \Rightarrow \left[S_{PP}(f)\right] = \begin{bmatrix} S_{11}(f) & S_{12}(f) & \cdots & S_{1P}(f) \\ S_{21}(f) & S_{22}(f) & \cdots & S_{2P}(f) \\ \vdots & \vdots & \ddots & \vdots \\ S_{P1}(f) & S_{P2}(f) & \cdots & S_{PP}(f) \end{bmatrix} \tag{15}$$

where $\Delta x = L_f / P$ is the flow-subjected tube region connected with each point force – and within which the turbulence excitation is tacitly assumed correlated. For obvious reasons, one should expect that $\Delta x < \lambda_c$ for adequate simulation of the random field.

Among the techniques developed following Shinozuka's original Cholesky decomposition of $[S_{PP}(f)]$, we will exploit here the elegant approach based on the Proper Orthogonal Decomposition (POD) of (15), also known as Karhunen-Loeve expansion. We wish to create partially correlated random signals $\{f_P(t)\}$ such that their Fourier transform $\{F_P(f)\}$ cope with (15). These signals are generated by mixing statistically independent signals $\{r_S(t)\}$, with Fourier transforms $\{R_S(f)\}$, so that :

$$\{F_P(f)\} = [M(f)]\{R_S(f)\} \tag{16}$$

where $[M(f)]$ are frequency dependent mixing matrices. Then, from (16), we obtain:

$$\{F_P(f)\}\{F_P(f)\}^H = [M(f)]\{R_S(f)\}\{R_S(f)\}^H [M(f)]^H \quad \Rightarrow \quad [S_{PP}(f)] = [M(f)][S_{SS}(f)][M(f)]^H \tag{17}$$

On the other hand, for each frequency f one may perform an eigen-decomposition of $[S_{PP}(f)]$:

$$[S_{PP}(f)][\Psi(f)] = [\Lambda(f)][\Psi(f)] \quad \text{with} \quad [\Psi(f)]^H [\Psi(f)] = [I] \tag{18}$$

where matrix $[\Lambda(f)] = Diag[\lambda_1(f), \lambda_2(f), ..., \lambda_L(f)]$ contains the $L = P$ eigenvalues of $[S_{PP}(f)]$, while the columns of $[\Psi(f)] \equiv [\{\psi_1(f)\}, \{\psi_2(f)\}, ..., \{\psi_L(f)\}]$ contain the corresponding eigenvectors. Because matrices $[S_{PP}(f)]$ are Hermitian positive-definite, their eigenvalues $\lambda_l(f)$ are always real and positive, while the eigenvectors $\{\psi_l(f)\}$ are in general complex. From (18) one can state the following relations:

$$[\Psi(f)]^H [S_{PP}(f)][\Psi(f)] = [\Lambda(f)] \quad \Rightarrow \quad [S_{PP}(f)] = [\Psi(f)][\Lambda(f)][\Psi(f)]^H \tag{19}$$

If we now build the mixing matrices $[M(f)]$ in (16) using the eigenvectors of $[S_{PP}(f)]$, we have:

$$[M(f)] \equiv [\Psi(f)] \quad \Rightarrow \quad \{F_P(f)\} = [\Psi(f)]\{R_S(f)\} \tag{20}$$

or, from (19) and (20):

$$[S_{PP}(f)] = [\Psi(f)][S_{SS}(f)][\Psi(f)]^H \quad \Rightarrow \quad [S_{SS}(f)] = \{R_S(f)\}\{R_S(f)\}^H = [\Lambda(f)] \tag{21}$$

Hence, $[\Lambda(f)]$ stand as cross-correlation matrices of the statistically independent signals $\{R_S(f)\}$, and are thus naturally diagonal. The preceding formulation supplies a convenient method for the generation of the partially correlated random forces $\{f_P(t)\}$. Using the Inverse Fourier Transform technique (with the number of time and frequency samples related as $N_T = 2K + 1$), the correlated forces arise as the sum of L independent principal component (POD) force terms:

$$\{f_P(t)\} = \sum_{l=1}^{L} \{f_P^l(t)\} = \frac{N_T}{\sqrt{2}} \sum_{l=1}^{L} FFT^{-1}\left(\{\sigma_{Pk}^l\} e^{-i\varphi_k^l} \; ; k = -K, ..., K\right) \tag{22}$$

with, for each force location $p = 1, 2, ..., P$ and each component $l = 1, 2, ..., L$, the spectral amplitudes:

$$\{\sigma_{Pk}^l\} = \{\psi_l(f_k)\}\{\sqrt{\lambda_l(f_k)\,\Delta f}\} \tag{23}$$

and using sampled random phases uniformly distributed in the range $\varphi_k^l \in [0 \; 2\pi]$, for each orthogonal component $l = 1, 2, ..., L$. Partial correlation of the forces $\{f_P(t)\}$ then stems from the superposition of the L terms $\{f_P^l(t)\}$. When all principal components are used, the number of independent signals generated equals the number of correlated point forces, $L = P$. However, if the order of magnitude of the eigenvalues $\lambda_l(f)$ in $[\Lambda(f)]$ decreases significantly with the POD component order, then the computation becomes more effective by truncating the number of principal components, so that $L < P$.

4.2 Simple method using a set of uncorrelated forces

The main and simple idea of the approach developed is to use a set of R uncorrelated point-forces located along the tube, which are generated with spectral properties and amplitudes such that they induce the same

linear modal responses as the original continuous formulation expressed by (11) or (13). For a set of P random *correlated* point forces $\{f_P(t)\} \equiv f(x_p,t)$ with $p=1,2,...,P$, the resulting modal responses read:

$$S_{q_nq_n}(f) = |H_n(f)|^2 \sum_{p=1}^{P}\sum_{r=1}^{P} \phi_n(x_p)\phi_n(x_r) S_f\left(x_p, x_r, f\right) \tag{24}$$

However, the same result may be obtained much easier assuming that the applied random force set is *uncorrelated*. Then (24) simplifies to:

$$S_{q_nq_n}(f) = |H_n(f)|^2 \sum_{p=1}^{P} |\phi_n(x_p)|^2 \Phi_p\left(x_p, f\right) \tag{25}$$

where $\Phi_p\left(x_p, f\right)$ is the auto-spectrum of the point force applied at location x_p.

We now enforce the condition that modal responses (11) or (13) and (25) be the same for all modes of interest. Then, using for instance (11) in the following:

$$\sum_{p=1}^{P} |\phi_n(x_p)|^2 \Phi_p\left(x_p, f\right) = \left(\frac{1}{2}\rho\bar{V}^2 D\right)^2 \frac{D}{\bar{V}}\bar{\Phi}\left(\frac{fD}{\bar{V}}\right) L_{cn}^2 \tag{26}$$

for modes $n=1,2,...,N$. Based on the previous simplifying assumptions, it is sensible to postulate the same spectral content $\Phi_{exc}(f)$ for the full set of equivalent point-forces. Furthermore, these should have amplitudes consistent with the local pressure head – in terms of the velocity profile $u(x_r)$ – so that we may write for all point-forces $p=1,...,P$:

$$\Phi_p\left(x_p, f\right) = B_p\, \Phi_{exc}(f) \quad \text{with} \quad B_p = A u(x_p)^4 \tag{27}$$

where $A>0$ is an unknown coefficient to be computed. Then, replacing (27) into (26), we obtain:

$$A\Phi_{exc}(f)\sum_{p=1}^{P}\left[u(x_p)^2\phi_n(x_p)\right]^2 = \left(\frac{1}{2}\rho\bar{V}^2 D\right)^2 \frac{D}{\bar{V}}\bar{\Phi}\left(\frac{fD}{\bar{V}}\right) L_{cn}^2 \tag{28}$$

for $n=1,2,...,N$. Identification of the frequency-dependent terms in (28) leads to the spectrum:

$$\Phi_{exc}(f) = \left(\frac{1}{2}\rho\bar{V}^2 D\right)^2 \frac{D}{\bar{V}}\bar{\Phi}\left(\frac{fD}{\bar{V}}\right) \tag{29}$$

while coefficient A must fulfil the following N conditions, whence the corresponding solution:

$$A\sum_{p=1}^{P}\left[u(x_p)^2\phi_n(x_p)\right]^2 = L_{cn}^2 \quad (n=1,2,...,N) \;\Rightarrow\; A = \begin{Bmatrix} \sum_{p=1}^{P}\left[u(x_p)^2\phi_1(x_p)\right]^2 \\ \sum_{p=1}^{P}\left[u(x_p)^2\phi_2(x_p)\right]^2 \\ \vdots \\ \sum_{p=1}^{P}\left[u(x_p)^2\phi_N(x_p)\right]^2 \end{Bmatrix}^{+} \begin{Bmatrix} L_{c1}^2 \\ L_{c2}^2 \\ \vdots \\ L_{cN}^2 \end{Bmatrix} \tag{30}$$

which is of the least-squares type, where $\{M\}^+$ is the Moore-Penrose pseudo-inverse of $\{M\}$. Once the parameters of the equivalent force set (27) have been obtained, each one of the statistically independent gaussian time-domain realizations $f_p(t) \equiv f(x_p,t)$, at the P point-forces, is generated using the standard Inverse Fourier Transform procedure:

$$f_p(t) = \frac{N_T}{\sqrt{2}}\sum_{l=1}^{L} FFT^{-1}\left(\sigma_k\, e^{-i\varphi_k}\,; k=-K,...,K\right) \tag{31}$$

using, for each force location $p=1,2,...,P$, sampled random phases uniformly distributed in the range $\varphi_k \in [0\ \ 2\pi]$ and the spectral amplitudes:

$$\sigma_k = \sqrt{\Phi_{exc}(f_k)\Delta f} \tag{32}$$

5 LINEAR COMPUTATIONS

Before dealing with the vibro-impact motions of gap-supported tubes, it will prove interesting to evaluate the preceding techniques on a single-span, linearly supported, tube. Linear modal response amplitudes can be inferred by frequency-integration of the response spectra (11), leading to the result:

$$\sigma_n^2 = \left(\frac{1}{2}\rho \bar{V}^2 D\right)^2 \frac{D}{\bar{V}} \bar{\Phi}\left(\frac{f_n D}{\bar{V}}\right) \frac{L_{cn}^2}{64\pi^3 m_n^2 f_n^3 \zeta_n} \quad (n = 1, 2, ..., N) \tag{33}$$

We now assume a pinned-pinned tube with length $L = 0.6$ m and diameter $D = 0.02$ m, presenting the following modal parameters: $m_n = 0.607$ kg $(\forall n)$, $f_n = 39n^2$ Hz, $\zeta_n = 1\%$ $(\forall n)$. The tube is subjected to a uniform cross-flow with $V = 3$ m/s and $\rho = 1000$ kg/m^3. For validation purposes, the following constant value of the *reduced spectrum* $\bar{\Phi}$ will first be used:

$$\bar{\Phi}(f_R) = 2.5\,10^{-2} \quad (\forall f_R) \tag{34}$$

together with the following postulated correlation length values: (a) $\lambda_c = 10D = 0.2$ m; (b) $\lambda_c = D = 0.02$. Then, from equation (33) and using the exact double integral (12) for computing L_{cn}^2, the theoretical responses of the first tube mode are given as: (a) $\sigma_1 = 0.70\,10^{-3}$ m; (b) $\sigma_1 = 0.25\,10^{-3}$ m.

5.1 General method using a set of partially correlated forces

Numerical simulations were performed by successively increasing the number of correlated point forces which simulate the turbulence field, in order to assert the adequate value of the "force density" as a function of the correlation length, $\Delta x/\lambda_c$. These are based on the time-step integration of the system modal equations (1) and (2), as detailed in Axisa et al (1988), using the partially correlated random excitation force set computed using (22) and (23), as explained in Section 4.1. The numerical results are based on 10 seconds of computed responses (about 400 cycles of the first tube mode).

Table 1. Linear response of the tube first mode to cross-flow turbulence excitation.

λ_c	**10 *D***					***D***				
P	**1**	**2**	**4**	**8**	**16**	**10**	**20**	**40**	**80**	**160**
Δx (m)	1.0	0.5	0.25	0.125	0.062	0.1	0.05	0.025	0.012	0.006
$\Delta x/\lambda_c$	**5**	**2.5**	**1.25**	**0.625**	**0.312**	**5**	**2.5**	**1.25**	**0.625**	**0.312**
$\sigma_1 \times 10^3$ (m)	1.75	0.91	0.76	0.72	0.71	0.40	0.30	0.26	0.25	0.25

The results obtained are presented in Table 1, for both cases $\lambda_c = 10D$ and $\lambda_c = D$. They clearly show the convergence of the method as the number of forces P increases, as well as the need for a minimum force density such that $\Delta x/\lambda_c \leq 1$, otherwise the excitation will display excessive spatial correlation. Notice that this physical constraint imposes a large number of point forces when L_f/λ_c is big, which is the usual case, meaning in practice that the computational effort to generate the random excitation force set may be quite significant (depending on the number of POD components used), even if compared with the effort needed for the numerical integration of the dynamical equations. Based in these results, for all following computations using this method, we will adopt $\Delta x/\lambda_c \leq 1$.

As a second example, consider the same tube subjected to a flow velocity profile of "triangular" shape, $V(x) = \bar{V}u(x)$, with $u(x) = 1 - (x/L)$ and $\bar{V} = 2$ m/s, see Figure 1(a). We will use, from now on, the following non-constant more realistic *reduced spectrum* $\bar{\Phi}$ – see Axisa et al (1990) – shown in Figure 1(b):

$$\bar{\Phi}(f_R) = \begin{cases} 2.5\,10^{-2} & f_R < 0.1 \\ 5\,10^{-5}\ f_R^{-2.7} & f_R \geq 0.1 \end{cases} \quad ; \quad f_R = \frac{fD}{V} \tag{35}$$

Figure 1(c) displays the full cross-correlation matrix $[S_{PP}(f)] \equiv [S_f(x_i, x_j, f)\,;\, i, j = 1, 2, ..., P]$ between the point forces, as computed from equation (15) using $\lambda_c = 10D$. One may notice the decrease of the (real) terms $S_{ij}(f)$, as they get farther from the matrix diagonal. Figure 2 illustrates the corresponding results from the POD decomposition of $[S_{PP}(f)]$, equation (18). One may notice the "spectral" shape of the principal components $\lambda_l(f)$, the eigenvalues of $[S_{PP}(f)]$, as well as the decrease of their magnitude as the component order $l = 1, 2, ..., L$ increases. Also notice that the corresponding eigenvectors $\{\psi_l(f)\}$ only display small changes with the frequency, which is often – although not always – the case.

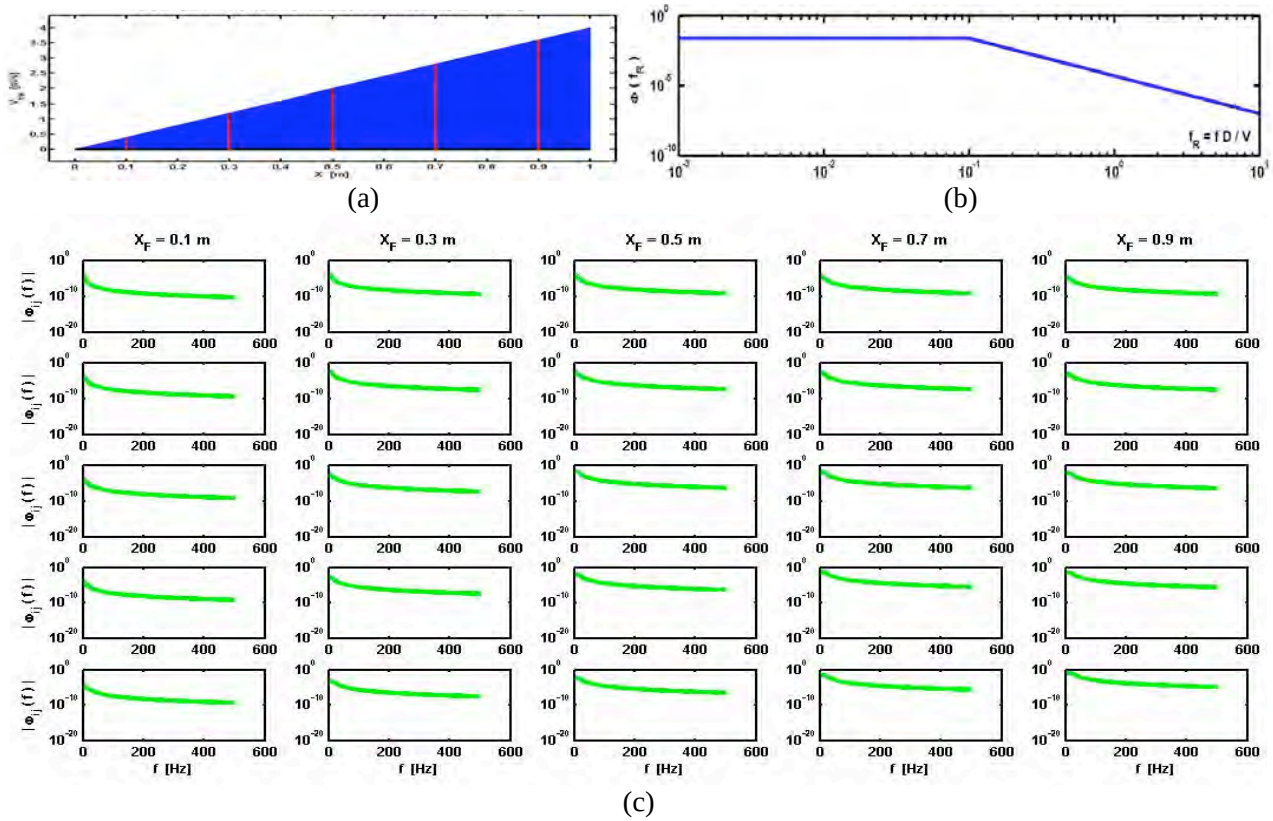

Figure 1. (a) Flow profile $V(x)$ and set of 5 point forces used in simulation; (b) Reduced excitation spectrum $\bar{\Phi}(f_R)$; (c) Cross-correlation matrix $S_{ij}(f)$ between the point forces, when $\lambda_c = 10D$.

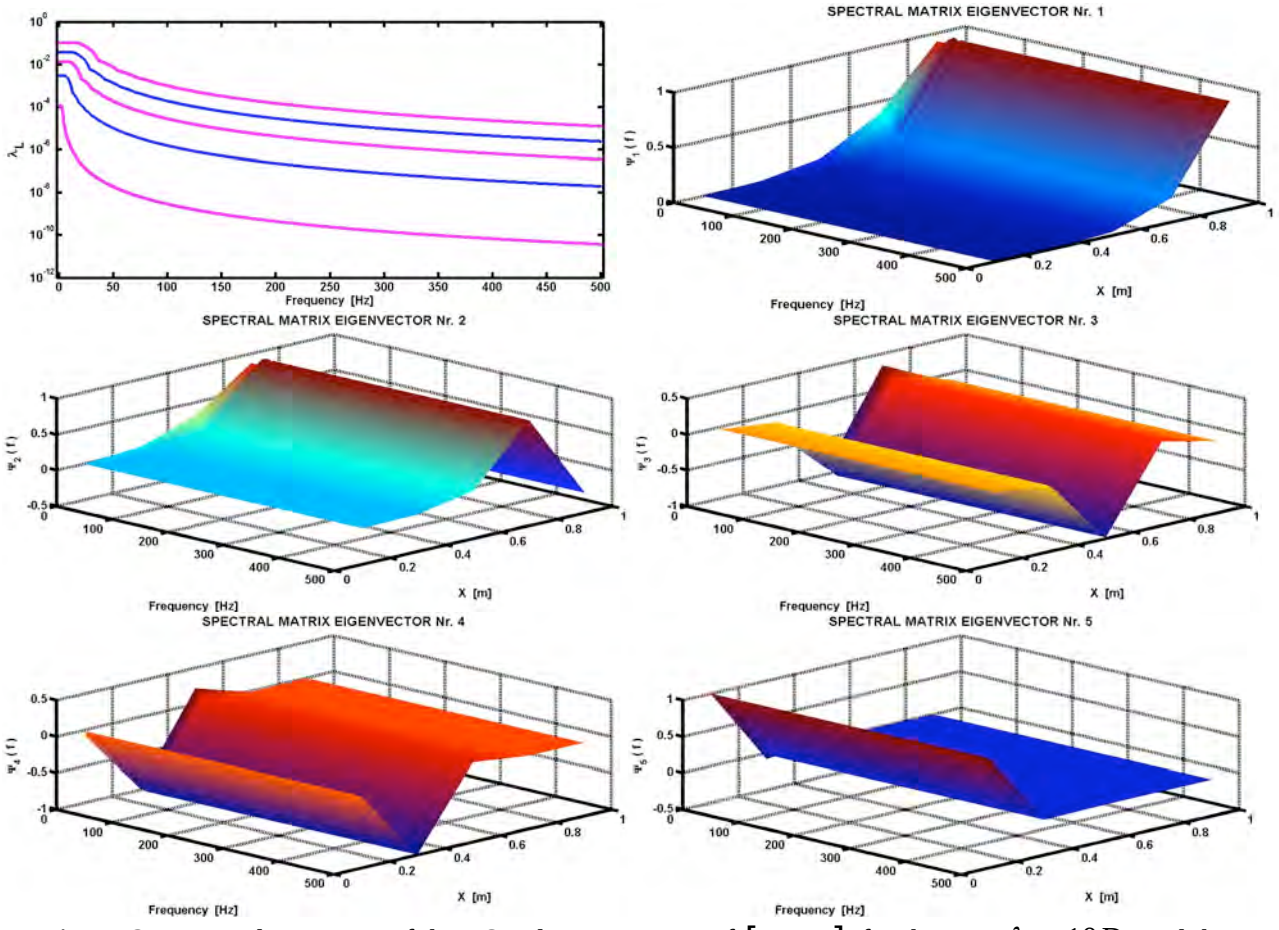

Figure 2. Eigenvalues $\lambda_l(f)$ of the POD decomposition of $[S_{PP}(f)]$, for the case $\lambda_c = 10D$, and their corresponding eigenvectors $\{\psi_l(f)\}$.

Figure 3(a) illustrates time-domain samples of the 5 random forces thus generated. The effects of the non-uniform velocity profile are clearly expressed in their amplitude, as well as through their frequency content. Figure 3(b) displays the cross-correlation coefficients between these forces, computed as:

$$C_{ij} = \frac{E\left\langle F_i(t)\, F_j(t)\right\rangle}{\sqrt{E\left\langle F_i(t)\, F_i(t)\right\rangle E\left\langle F_j(t)\, F_j(t)\right\rangle}} \tag{36}$$

where $E\langle G(t)\rangle$ is the mathematical expectation of $G(t)$ as $t \to \infty$. These coefficients highlight a correlation decrease as their distance augments and confirm that the forces have been correctly generated.

Figure 4 illustrate the 2-dimensional tube response computed at location $x_r = 0.45L$, using the reduced spectrum (35) and $\lambda_c = 10D$, the tube dynamics being modelled through 6 modes. For future comparison, the numerical RMS response amplitudes obtained were: (a) $\sigma_r = 0.35\,10^{-3}$ m for $\lambda_c = 10D$; (b) $\sigma_r = 0.14\,10^{-3}$ m for $\lambda_c = D$. In this last case, 50 point forces were used to simulate the excitation field.

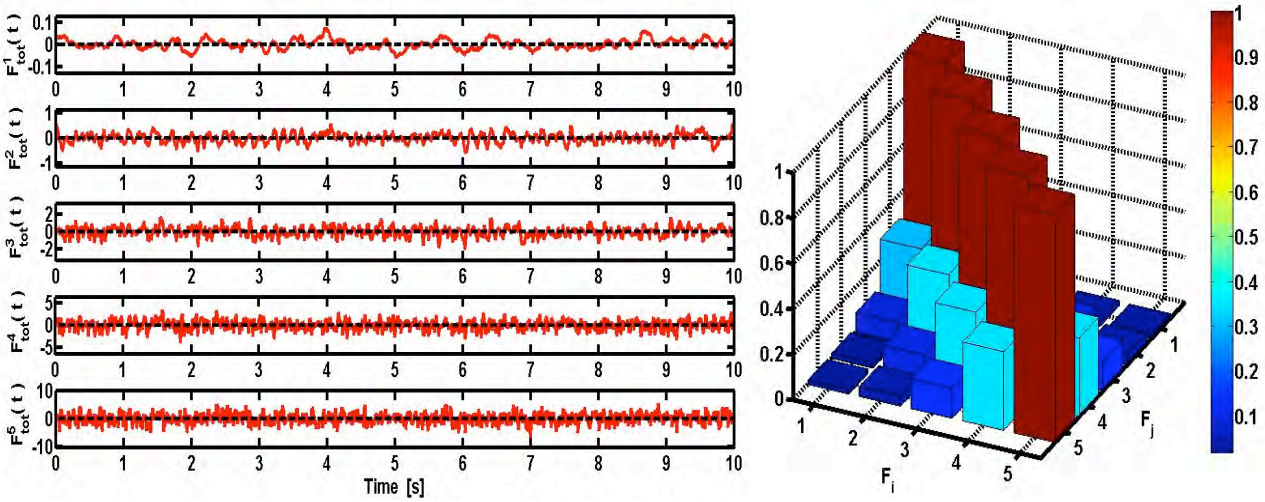

Figure 3. (a) Time-domain samples of the 5 partially correlated random forces; (b) Correlation coefficients.

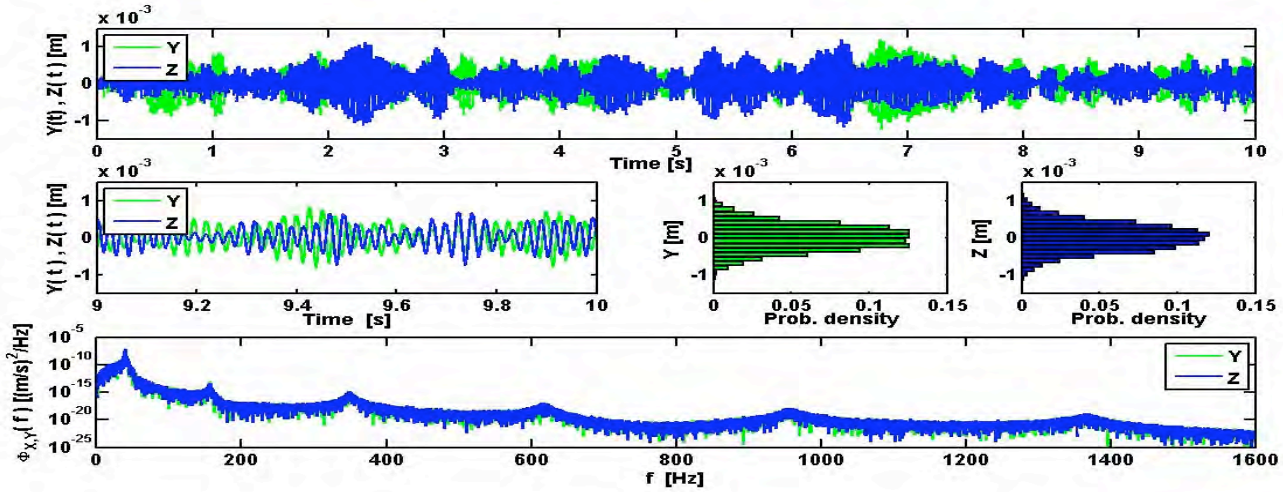

Figure 4. Computed tube response at location $x_r = 0.45L$ ($\lambda_c = 10D$).

5.2 Simple method using a set of uncorrelated forces

Returning to the first example with a uniform velocity profile and the constant reduced spectrum (34), computations performed using the simplified method for excitation generation led to the following numerical response amplitudes of the first tube mode: (a) $\sigma_1 = 0.78\,10^{-3}$ m for $\lambda_c = 10D$; (b) $\sigma_1 = 0.25\,10^{-3}$ m for $\lambda_c = D$. as can be seen, these values are totally compatible with those obtained from the general method. A slightly

higher magnitude is now obtained, for the case $\lambda_c = 10D$, because of the use of the simplified correlation integral (12), which overestimates L_{cn}^2 as λ_c / L_f increases.

Notice however that the excitation generation using the simplified method is much more efficient than the general method. Actually, because only the first mode is of interest in these computations, a single random force is enough to simulate the effects of the turbulence field, irrespective of the value of λ_c / L_f. The general excitation generation method is noticeable more greedy in computational resources and workload – by one or two orders of magnitude – a conclusion extensive to other computations in this paper.

We now turn to the second example, with a non-uniform velocity profile. Figure 5 shows, as a function of the number P of point forces used, the global error in reconstructing the theoretical linear modal responses, as computed from the following equation:

$$\Delta^2 = \sum_{n=1}^{N} \left[\left(\sum_{p=1}^{P} \left[u(x_p)^2 \phi_n(x_p) \right]^2 \right) A - L_{cn}^2 \right]^2 \tag{37}$$

which is the error inferred from the least-squares solution (30). The result shown is typical, in that Δ becomes irrelevant for all values $P > N$, meaning that the number of point forces needed is usually equal or only slightly higher than the number of modes used in the computation. Indeed, we showed in Antunes at al (2008) that further increasing the number of point forces does not bring any changes in the computed responses, which demonstrates the robustness of the excitation method.

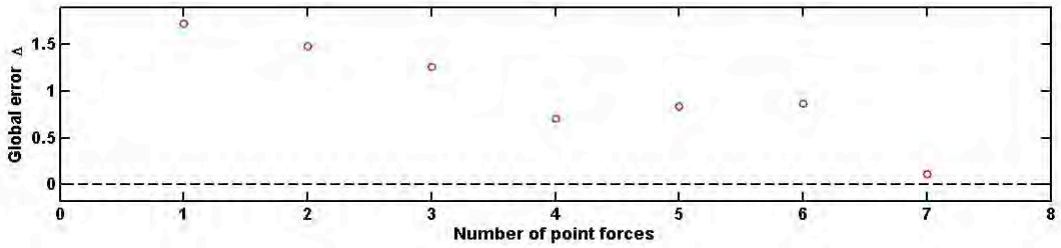

Figure 5. Global error on the linear modal responses as a function of the number P of point forces.

The responses obtained from the time-domain simulations are the following : (a) $\sigma_r = 0.48\,10^{-3}$m for $\lambda_c = 10D$; (b) $\sigma_r = 0.15\,10^{-3}$m for $\lambda_c = D$. The first result is about 30% higher than the response obtained using the general method of excitation, while the second result is virtual identical using both approaches. Theoretical computations using equation (33) confirmed that the difference obtained in the case $\lambda_c = 10D$ stems mostly from the use of the approximate formula when computing the joint acceptances L_{cn}, instead of the exact one – see equations (12). This is well illustrated by the values shown in Table 2.

Table 2. Correlation integrals (joint acceptances).

λ_c	**10 *D***					***D***				
n	**1**	**2**	**3**	**4**	**5**	**1**	**2**	**3**	**4**	**5**
L_{cn} exact	0.51	0.55	0.47	0.39	0.33	0.19	0.24	0.24	0.24	0.24
L_{cn} approximate	0.60	0.75	0.78	0.79	0.79	0.19	0.24	0.25	0.25	0.25

Therefore, a more exact response amplitude could be easily obtained for $\lambda_c = 10D$ if the exact joint-acceptances were used when computing the point forces through (30). Such differences are however irrelevant, as in practice λ_c is quite small, so the approximate integral is usually adequate.

For non-uniform flows, an important difference between the two approaches is the fact that the reduced frequencies and reduced spectra – equation (9) – are processed in the general method using the true local velocities $V(x_p)$, while in the simplified method the average velocity $\overline{V}$ is used everywhere. For some extreme flow configurations, this may obviously entrain some errors. As a final remark notice that, due to the non-uniform velocity profile $u(x)$, the amplitude coefficients become in this configuration quite significant for the higher order modes.

6 NONLINEAR GAP-SUPPORTED TUBES

Due to lack of space, results from a single multi-supported tube configuration will be presented here. A tube similar to the one previously used, but with length $L = 2\,\text{m}$ and three equidistant intermediate gap-supports with clearances $\delta_s = \pm 0.1\,\text{mm}$, is subjected to the *uniform* (with $\overline{V} = 3\,\text{m/s}$) and *non-uniform* (with $0 \le V(x) \le 4\,\text{m/s}$) flows shown in Figure 6. Reduced spectrum (35) is used, together with a correlation length $\lambda_c = D$. The mid-span amplitudes and average contact/impact forces at the gap-supports are computed using both methods of excitation generation. Dynamical modelling was performed for 10 seconds using 20 modes.

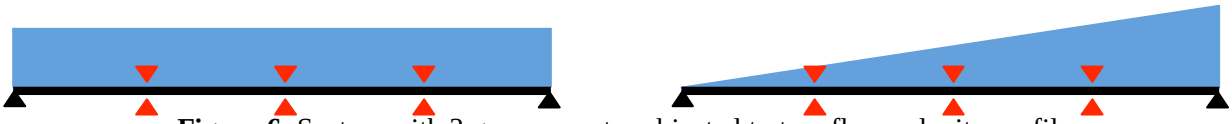

Figure 6. System with 3 gap-supports subjected to two flow velocity profiles.

Table 3. Results of the nonlinear computations.

Method	**General method using a set of partially correlated point forces**	**Simple method using a set of uncorrelated point forces**
Number of point forces	**100**	**21**
$\sigma_r \times 10^5$ at mid-span (m)	**(a)** 5.21 7.18 7.14 5.19	**(a)** 5.22 7.06 7.09 5.20
$\overline{F_c}$ at gap-support (N)	**(a)** 1.30 1.37 1.30	**(a)** 1.25 1.25 1.22
$\sigma_r \times 10^5$ at mid-span (m)	**(b)** 4.59 6.41 6.47 4.57	**(b)** 4.96 6.51 6.72 5.08
$\overline{F_c}$ at gap-support (N)	**(b)** 0.61 0.64 0.60	**(b)** 0.83 0.82 0.97

The results obtained are shown in Table 3. They are near-similar for the uniform velocity, while for the triangular profile the simple method comparatively over-excites moderately the tube. However, within reasonable bounds, these results suggest that our simple method of excitation generation is adequate (although eventually somewhat conservative) when addressing nonlinear vibro-impact computations.

7 CONCLUSION

In this paper we confronted two methods for the generation of force sets which simulate the random excitation of turbulent flow fields. For all practical purposes, both techniques proved reasonably equivalent, for both linear and nonlinear conditions, uniform and non-uniform flows. However, the general method based on Shinozuka's work is much more resource-consuming than our structure-dependent simple method.

REFERENCES

Antunes, J., Delaune, X., Piteau, P., Borsoi, L. 2008. A simple consistent method for the time-domain simulation of turbulence excitations applied to tube/support dynamical analysis under non-uniform flows. *9th Int. Conference on Flow-Induced Vibrations* (FIV2008), 30 June - 3 July 2008, Prague.

Axisa, F., Antunes, J., Villard, B. 1988. Overview of numerical methods for predicting flow-induced vibrations. ASME Journal of Pressure Vessel Technology. Vol. 110. P 6-14.

Axisa, F., Antunes, J., Villard, B. 1990. Random excitation of heat-exchanger tubes by cross-flows. Journal of Fluids and Structures. Vol. 4. P 321-341.

Fisher, N., Olesen, M., Rogers, R., Ko, P. 1989. Simulation of tube-to-support dynamic interaction in heat exchange equipment. ASME Journal of Pressure Vessel Technology. Vol. 111. P 378-384.

Haslinger, K., Steininger, D. 1995. Vibration response of a U-tube bundle with anti-vibration bar supports due to turbulence and fluidelastic excitations. Journal of Fluids and Structures. Vol. 9. P 805-834.

Hassan, M., Weaver, D., Dokainish, M. 2003. The effects of support geometry on the turbulence response of loosely supported heat exchanger tubes. Journal of Fluids and Structures. Vol. 18. P 529-554.

Sauvé, R., Teper, W. 1987. Impact simulation of process equipment tubes and support plates – a numerical algorithm. ASME Journal of Pressure Vessel Technology. Vol. 109. P 70-79.

Shinozuka, M. 1971. Simulation of multivariate and multidimensional random processes. Journal of the Acoustical Society of America. Vol. 49. P 357-367.

Shinozuka, M., Yun, C., Seya, H. 1990. Stochastic methods in wind engineering. Journal of Wind Engineering and Industrial Aerodynamics. Vol. 36. P 829-843.